ACS APPLIED MATERIALS & INTERFACES

Research Article

www.acsami.org

Photo-Cross-Linkable Methacrylated Gelatin and Hydroxyapatite Hybrid Hydrogel for Modularly Engineering Biomimetic Osteon

Yicong Zuo,† Xiaolu Liu,† Dan Wei, Jing Sun, Wenqian Xiao, Huan Zhao, Likun Guo, Qingrong Wei, Hongsong Fan,* and Xingdong Zhang

National Engineering Research Center for Biomaterials, Sichuan University, Chengdu, Sichuan 610064, People's Republic of China

Supporting Information

ABSTRACT: Modular tissue engineering holds great potential in regenerating natural complex tissues by engineering three-dimensional modular scaffolds with predefined geometry and biological characters. In modular tissue-like construction, a scaffold with an appropriate mechanical rigidity for assembling fabrication and high biocompatibility for cell survival is the key to the successful bioconstruction. In this work, a series of composite hydrogels (GH0, GH1, GH2, and GH3) based on a combination of methacrylated gelatin (GelMA) and hydroxyapatite (HA) was exploited to enhance hydrogel mechanical rigidity and promote cell functional expression for osteon biofabrication. These composite hydrogels presented a lower swelling ratio, higher mechanical moduli, and better biocompatibility when compared to the pure GelMA hydrogel. Furthermore, on the basis of the composite hydrogel and photolithograph technology, we successfully constructed an osteon-like concentric double-ring structure in which the inner ring encapsulating human umbilical vascular endothelial cells (HUVECs) was designed to imitate blood vessel tubule while the outer ring encapsulating human osteoblast-like cells (MG63s) acts as part of bone. During the coculture period, MG63s and HUVECs exhibited not only satisfying growth status but also the enhanced genic expression of osteogenesis-related and angiogenesis-related differentiations. These results demonstrate this GelMA−HA composite hydrogel system is promising for modular tissue engineering.

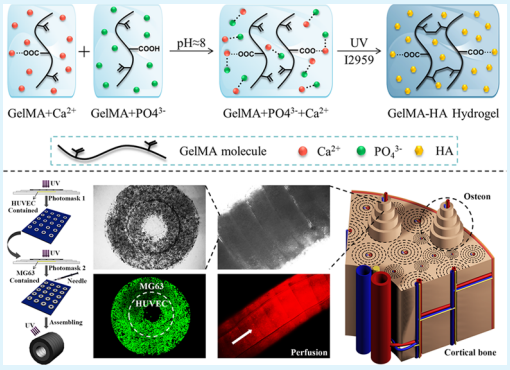

KEYWORDS: *methacrylated gelatin, hydroxyapatite, modular tissue engineering, osteon*

1. INTRODUCTION

Modular tissue engineering has emerged as a promising field to regenerate an intricate microenvironment and cellular-scale precision of natural tissues by assembling microscale modules with specific architectural and biological features into desirable macroscale constructs over the last few decades. It possesses great prospective potential to exceed traditional tissue engineering which often has difficulty regenerating complex natural tissues.[1]

One of the crucial challenges in modular tissue engineering is to prepare appropriate microscale modules. Various methods have been employed to create these modules, such as cellular self-assembly,[2] microfabrication of cell-laden hydrogels,[3] creation of cell sheets,[4] and three-dimensional (3D) cell printing.[5] Among these ways, microgels are popular due to their high content of physiological fluids and biomimetic nature emulating the native extracellular matrix (ECM).[6] One remarkable example of fabricating these microgel-based modules comes from the usage of the photo-cross-linkable material by bottom-up assembly.[7] This approach offers us a rapid and scalable manufacture of modular constructs with predefined geometrical and biological characters. In the past years, this bottom-up assembly has had reasonable progress and it has been found that the mechanical property and biocompatibility of the hydrogel are the most important two factors which can influence the microarchitecture, block assembly, and cell behaviors.[8,9]

However, most hydrogels applied have obstacles to meet both requirements. Due to the inherent rigid mechanical property and micropattern fidelity, poly(ethylene glycol) diacrylate (PEGDA) or poly(ethylene glycol) dimethacrylate (PEGDMA) has been mostly applicable to construct microgel modules.[3,10] In most cases these PEG hydrogels always failed the cell trials, in which dramatically decreased cell viabilities over time and inhibited cell−matrix responsive behaviors were observed.[11] This mainly comes from the lack of cell binding motifs as well as poor polymer network degradation in PEG.[12] Therefore, many other novel photo-cross-linkable hydrogels derived from those used in traditional tissue engineering have been exploited, such as collagen,[13] alginate,[14] and gelatin.[15] Among these materials, methacrylated gelatin (GelMA) emerges as a prominent candidate because of its outstanding biocompatibility, anti-inflammation, and cost efficiency. Nonetheless, the weakness of mechanical rigidity associated with

Received: February 13, 2015
Accepted: April 29, 2015
Published: April 30, 2015

DOI: 10.1021/acsami.5b01433
ACS Appl. Mater. Interfaces 2015, 7, 10386−10394

GelMA hydrogel greatly limits its applications in microscale construction and modular assembly.[15] Hence, exploration of a hydrogel material with appropriate mechanical property for benefiting the modular assembly and high biological activities for cell cultivation is of great significance. To achieve this goal, preparation of a multi-ingredient hydrogel system can be a foreseeing strategy. In particular, for specific tissue construction, it is generally of help that a biomimetic matrix is created based on a comprehensive recognition of physical compositions and in vivo formation process of the target tissue.

Cortical bone is comprised of the repeating functional osteon units;[16] thus, it is a typical example of native tissue which can be reconstructed by modular tissue engineering. To achieve a structural and functional mimicking, biofabrication of osteon-like modular scaffolds would be vital. As to the microscale structure, osteon is a highly vascularized tissue with a unique concentric double-ring structure which can offer us a modular design. Besides its structural character, a look at the bone compositions under the nanoscale level shows us an inspiring combination system of collagen fiber and mineralized hydroxyapatite (HA).[16] This organic−inorganic composite is the typical feature of bone matrix. With increasing understanding of the bone matrix formation mechanism in vivo, plenty of attempts have been made to construct similar biomimetic systems by precipitating HA into synthetic polymer templates or natural ones. Significantly, these fabricated composites have been demonstrated to facilitate cell−cell, cell−matrix responses to stimulate osteogenesis.[17,18] However, most of these template materials are based on preshaped scaffolds without the ability to realize in situ cell encapsulation and modular construction. To overcome this shortcoming, employing a photo-cross-linkable hydrogel as the substrate could be a potent solution.

As mentioned above, although mechanically weak, GelMA hydrogel is a superior selection since it is photo-cross-linkable and contains gelatin as backbone while inheriting its natural advantages. In particular, gelatin is the main product of collagen hydrolysis and retains chemical and biological features of collagen which provide cell-responsive characteristics, cell adhesion sites, and proteolytic degradability, for example.[15] Furthermore, as the mainly inorganic composite of natural bone matrix, HA has been proved to be bioactive to guide and induce bone formation;[19] therefore, HA-precipitated GelMA hydrogel might provide improved cell−matrix responses to enhance bone-related cell functional expression. This potential has been partially proved by previous studies about the gelatin−HA composite scaffold for bone tissue engineering.[20,21] In addition, the precipitation of HA into GelMA network might also strengthen the whole mechanical rigidity of GelMA hydrogel, which would be in favor of modular assembly.

On the basis of the above descriptions, we herein attempt to demonstrate the novel example of the preparation of GelMA−HA composite hydrogel with enhanced mechanical rigidity and bioactivity. The physicochemical properties of the composite as well as cellular responses within the 3D network of the bulk hydrogel were characterized. Subsequently, we investigated the feasibility of this GelMA−HA material in generating modular systems for constructing biomimetic osteon.

2. MATERIALS AND METHODS

2.1. Materials. The UV light source (OmniCure S1500) was purchased from EXFO Photonic Solutions Inc. Gelatin (Porcine Type A, Cat No. G2500), methacrylic anhydride, 2-hydroxy-4′-(2-hydroxyethoxy)-2-methylpropiophenone (I2959), fluorescein diacetate (FDA), and propidium iodide (PI) were obtained from Sigma-Aldrich (USA). Photomasks were designed by AutoCAD 2007 and printed by Qingyi Precision Maskmaking Co. Ltd. Unless otherwise stated, all other reagents were obtained from Chengdu Kelong Chem Co.

2.2. GelMA−HA Composite Hydrogel Preparation. *2.2.1. GelMA Synthesis.* GelMA was synthesized as given in the previous report.[8] In brief, gelatin (10 g) powder was dissolved in 100 mL of Dulbecco's Phosphate Buffered Saline (DPBS) under 50 °C, and methacrylic anhydride (10 mL) was added slowly. The mixture was stirred for 3 h under 50 °C and then diluted with 500 mL of DPBS. Lastly, the solution was dialyzed against distilled water, which was changed twice a day at 37 °C for 1 week, using a 12−14 kDa dialysis tube. The final solution was freeze dried to a constant weight, and the gained GelMA solid was stored at room temperature.

2.2.2. Preparation of GelMA−HA Serial Prepolymer Solution. GelMA−HA solutions were prepared from GelMA, $CaCl_2$, and Na_2HPO_4. The Ca and P precursors were dissolved separately at a ratio of Ca/P = 1.67 in equivalent distilled water, including 0.5 w/v % I2959. An equal amount of GelMA was added to each solution and stirred until they were completely dissolved under 37 °C at a concentration of 10 w/v %. Then the GelMA−P solution was added to GelMA−Ca dropwise, and NaOH was used to adjust the pH of the mixed solution to approximately 8. The final GelMA−HA solution was gained by being stirred at 37 °C for 24 h and stored at room temperature. In addition, varying the quantity of Ca and P (maintain the same 1.67 ratio) can form different HA-containing groups: 0, 1, 2, and 3 w/v % (GH0, GH1, GH2, and GH3); the w/v % was calculated by $W_{HA}/V_{Solution} \times 100\%$.

2.2.3. Preparation of GelMA−HA Bulk Hydrogel. The GelMA-based solution was made into a hydrogel disc by using a circular Teflon mold measuring 8 mm in diameter and 2.4 mm in thickness (Figure S1, Supporting Information). After injecting the solution into the mold, gelation was induced by 10 s of ultraviolet (UV) exposure. Each hydrogel disc was in a cylinder shape with a diameter of 8 mm and a height of 2.4 mm.

2.2.4. Preparation of GelMA−HA Microgel and Assembly. As shown in Figure S2, Supporting Information, 150 μL of GelMA−HA prepolymer solution was pipetted on a glass slide, on which three spacer slides (each with a thickness of 150 μm) were placed on two sides to control the microgel height, and then another slide was put on slightly to cover the solution. Subsequently, photomask 1 was placed on the top and the inner-ring microgel was formed by 25 s of UV exposure (360−480 nm; 7.9 mW/cm^2). Afterward, the microgel-attached glass slide was rinsed with DPBS to remove the residue and utilized again to cover another prepolymer, on which photomask 2 was placed. The outer-ring gelation was induced by a second 25 s UV exposure. Last, the double-ring microgel unit was manually stripped from the glass and assembled one by one into a hollow tube which was stabilized by 5 s of UV lighting.

2.3. Characterization of the GelMA−HA Hydrogel. *2.3.1. X-ray Diffraction and Fourier Transform Infrared Spectroscopy Detection.* The phase composition and chemical bonding structure of GelMA−HA composite was analyzed by X-ray diffraction (XRD; Dandong Fangyuan DX-1000 diffractometer) and Fourier transform infrared spectroscopy (FTIR; PerkinElmer Spectrum one (B) spectrometer). The hydrogel disc samples for XRD and FTIR (Φ 8 mm × 2.4 mm) were freeze dried under vacuum and then tested at room temperature.

2.3.2. Transmission Electron Microscopy (TEM). The TEM image to show HA morphology and distribution was acquired using a transmission electron microscope (TecnaiG2F20S-TWIN, USA) at an accelerating voltage of 120 kV. Samples for TEM observation were prepared by dropping 10 μL of diluted GelMA−HA solution onto 400-mesh carbon-coated copper grids. High-resolution TEM (HRTEM) measurement was performed to show the internal structure of HA by using a TEM system operated at an acceleration voltage of 200 kV. The crystal pattern of HA was analyzed by selected area electron diffraction (SEAD).

DOI: 10.1021/acsami.5b01433
ACS Appl. Mater. Interfaces 2015, 7, 10386−10394

2.3.3. Scanning Electron Microscopy (SEM). For morphology observation of hydrogel internal network, the hydrogel discs (Φ 8 mm × 2.4 mm) were lyophilized after being initially frozen by liquid nitrogen and then placed in the E-1010 ION SPUTTER for gold coating. The final gold-coated samples were imaged by field emission scanning electron microscopy (FE-SEM, Hitachi S-4800) at 5 kV. The energy-dispersive spectroscopy (EDS) system was used for recording the element distribution maps and calculating the Ca/P ratio.

2.3.4. Swelling Experiment. To test the swelling behavior of the hydrogels, each hydrogel disc (Φ 8 mm × 2.4 mm) was immersed in 1 mL of DPBS with a constant temperature of 37 °C. At each time point of 1, 2, 4, 8, 12, and 24 h, the discs were removed for wet weight (W_1) recording, before which the surface water of the hydrogel was quickly removed using filter paper. The weight of each hydrogel before immersion was recorded as W_0. Calculation of the swelling ratio was based on the following formula: $(W_1 - W_0)/W_0$. Three parallel samples per group were measured.

2.3.5. Mechanical Tests and Assembly Performance of the GelMA-Based Hydrogel. The electromechanical universal testing machine (CMT 4104, Shenzhen SANA Testing Machine Co. LTD) was used to detect the compressive moduli of the hydrogel disc (Φ 8 mm × 2.4 mm). The compressive stress−strain was obtained at a strain rate of 1 mm/min under room temperature. According to the stress−strain curve, the compressive moduli were defined as the slope of the linear region from 0 to 10% strain. Three replicates were tested for each group.

The assembly performance of GH0, GH1, GH2, and GH3 was tested by sequentially assembling their microgels. The procedure was described in section 2.2.4. The final structure was imaged by a digital camera. The numbers of the unit in the assembly were used to evaluate the assembly performance.

2.4. Cell Culture and 3D Encapsulation. Human umbilical vascular endothelial cells (HUVECs) and human osteoblast-like cells (MG63s) were obtained from CCTCC (China Center for Type Culture Collection).

HUVECs (or MG63s) culture was maintained in a physiological condition at 37 °C in a humidified 5% CO_2−95% air atmosphere and cultured in high glucose DMEM (Gibco, USA) containing 10% fetal bovine serum and 1% penicillin/streptomycin. The culture medium was refreshed every 2−3 days, and cells were passaged twice a week. To prepare cell-laden hydrogel, cells were trypsinized, counted, centrifuged, and gently mixed in the prepolymer solution with a final concentration of 5×10^6 cells/mL (GH0, GH1, GH2, and GH3), and then the cell-containing prepolymers were gelled as in sections 2.2.3 or 2.2.4.

2.5. Cell Proliferation and Morphology in 3D GelMA-Based Bulk Hydrogel. Cell proliferation and morphologies in GH0, GH1, GH2, and GH3 bulk hydrogels were detected by MTT assay and FDA/PI staining. The predetermined time point for detection was 1, 4, and 7 days. In MTT test, cell-laden hydrogels were first immersed in DPBS containing 0.5 mg mL^{-1} MTT at 37 °C. After 4 h incubation, DPBS was removed and dimethyl sulfoxide (DMSO) was subsequently added to dissolve the purple formazan salts. Lastly, the multidetection microplate reader (Bio-Rad 550) was used to measure the absorbance of the solution at 490 nm. Three replicates per group were tested. For cell morphology observation, the samples were immersed in FDA/PI-containing DPBS for 1 min and then retrieved and imaged using the confocal laser scanning microscope (CLSM, Leica-TCS-SP5).

2.6. Characterization of Cell-Laden Osteon-Like Modules in Use of GelMA−HA Composite and Perfusion Test. The cell-laden microgel and assembly were prepared as described in section 2.2.4, in which the MG63s and HUVECs were encapsulated in the outer ring and inner ring of the osteon-like module, respectively, at a density of 5×10^6 cells mL^{-1}. The cell-laden unit and assembly was stained with FDA/PI and imaged by CLSM to observe cell growth and distribution. To test the connectivity of the assembled tube, Rhodamine B solution was pumped into the assembly at a rate of 5 μL min^{-1}, and the process was visualized under fluorescent microscopy (Leicactr 4000).

2.7. Cell Gene Expression. Osteogenesis-related and angiogenesis-related gene expression in osteon-like assembly was examined by quantitative real-time reverse transcriptase−polymerase chain reaction (qRT−PCR). Total RNA was extracted from each sample after 4 and 7 days using Trizol reagent (Invitrogen, USA) and then converted into complementary DNA (cDNA) via a ReverTra Ace qPCR RT Kit (Toyobo, Japan). The sequences of primers for collagen I (COL-I), osteocalcin (OCN), alkaline phosphatase (ALP), vascular endothelial growth factor (VEGF), and GAPDH genes are given in Table 1. The CFX96TM real-time PCR detection system (Bio-Rad, CFX960) with SsoFastTM EvaGreen Supermix (Bio-Rad) was used to perform the quantitative real-time PCR reaction. GAPDH as the housekeeping gene was utilized to normalize results. The relative expression values were calculated by the ΔΔCt value method. Each sample was averaged from three parallels.

Table 1. Primer Sequences Used for qPCR

symbol	primers
GAPDH	5′-GGCATGGACTGTGGTCATGAG-3′
	5′-TGCACCACCAACTGCTTAGC-3′
alkaline phosphatase	5′-GCTGGCAGTGGTCAGATGTT-3′
	5′-CTATCCTGGCTCCGTGCTC-3′
collagen type i	5′-CACACGTCTCGGTCATGGTA-3′
	5′-AAGAGGAAGGCCAAGTCGAG-3′
osteocalcin	5′-TTGGACACAAAGGCTGCAC-3′
	5′-CTCACACTCCTCGCCCTATT-3′
vascular endothelial growth factor	5′-TTGCCTTGCTGCTCTACCTCCA-3′
	5′-GATGGCAGTAGCTGCGCTGATA-3′

2.8. Statistical Analysis. Mean ± standard deviation (SD) was used to express all results. Statistical significance was examined by one- and two-way of variance (ANOVAs) and set at $p < 0.05$.

3. RESULTS

3.1. Characterization of GelMA−HA Composites.

3.1.1. XRD, FTIR, and TEM Analyses. The characteristic XRD and FTIR spectra of the GelMA−HA hydrogel are shown in Figure 1A and 1B. Data from GH2 was chosen as a representative sample. As can be seen from Figure 1A, comparing with GH0, the peaks (002, 211, 310, 222, and 213) observed in GH2 were typical from HA apatite. Also, the typical diffraction peaks of 002 and 211 appeared broadened.

The FTIR spectra in Figure 1B showed the chemical bands related to phosphate groups, particularly PO_4 (970, 605, and 567 cm^{-1}), which could be only attributed by apatite. Additionally, the typical bands in GH0, such as amide bands, were also observed in GH2 sample.

The TEM photo in Figure 1C showed that HA had a flake shape with a submicro/nanosize and dispersed well in GelMA solution. Both the HRTEM image and the SEAD pattern (Figure 1D) confirmed that HA was crystalline; the 0.028 and 0.034 nm spacings agreed well with the (211) and (002) lattice spacings of hexagonal HA.

3.1.2. SEM. A similar internal porous network was observed in all GelMA-based hydrogels as indicated in Figure 2. For GH0, the wall of GelMA was smooth, while in the HA-precipitated GelMA network, all three groups (GH1, GH2, and GH3) exhibited a rough wall.

Additionally, with increasing ratio of HA, there were little differences among the wall of all GelMA−HA samples. As shown in Figure S3, Supporting Information, for GH1, -2, and -3 samples, the elemental map of Ca and P showed a

DOI: 10.1021/acsami.5b01433
ACS Appl. Mater. Interfaces 2015, 7, 10386−10394

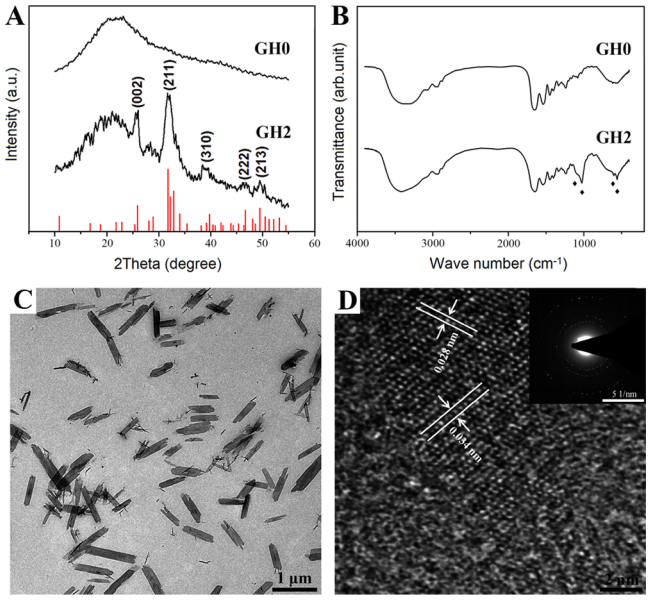

Figure 1. Characterization of GelMA-based composite: (A) XRD graph, (B) FTIR spectrum (phosphate-related bonds of PO_4 were noted by the star symbol), (C) TEM image for GH2, and (D) HRTEM of an individual HA in GH2; (inset) corresponding SEAD pattern.

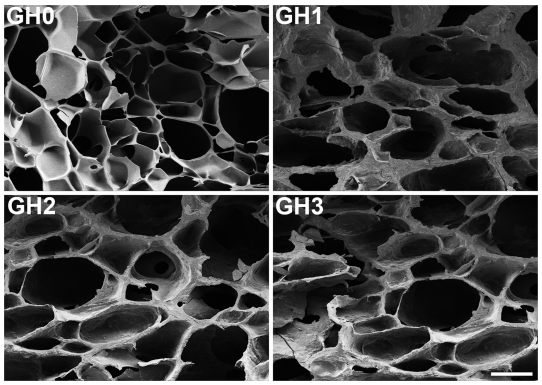

Figure 2. SEM images of cross-section of the composite hydrogels: GH0, GH1, GH2, and GH3. Scale bars: 100 μm.

homogeneous distribution along the network and the Ca/P ratio was 1.71, 1.61 and 1.78, respectively.

3.1.3. Swelling Experiment. Figure 3 depicts the swelling properties of the GelMA−HA hydrogels. A dramatic swelling was observed from 0 to 2.5 h in GH0, and the swelling tended to decrease after 5 h and reached saturation with an equilibrium swelling ratio of approximately 280% after 12.5 h. As for the other three tested groups (GH1, GH2, and GH3) with different precipitation ratios of HA, the swelling ratio was reduced significantly, maintaining the saturation level of 100% after 12.5 h. In addition, there was no obvious difference among the three groups.

3.1.4. Mechanical Tests and Assembly Performance. The mechanical properties of the hydrogels are shown in Figure 4A. The compressive modulus of GH0 hydrogel was ~13 kPa. With incorporation of 1w/v % HA, GH1 gained a little higher modulus of approximately 15 kPa. When the incorporation ratio of HA was increased to 2 and 3 w/v %, significantly higher moduli were exhibited by GH2 (~23 kPa) and GH3 (~24 kPa) with no significant difference between each other.

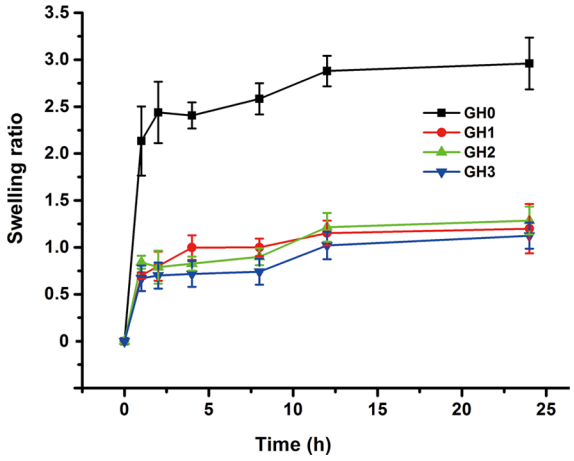

Figure 3. Swelling kinetics of the GelMA-based hydrogels in PBS under 37 °C.

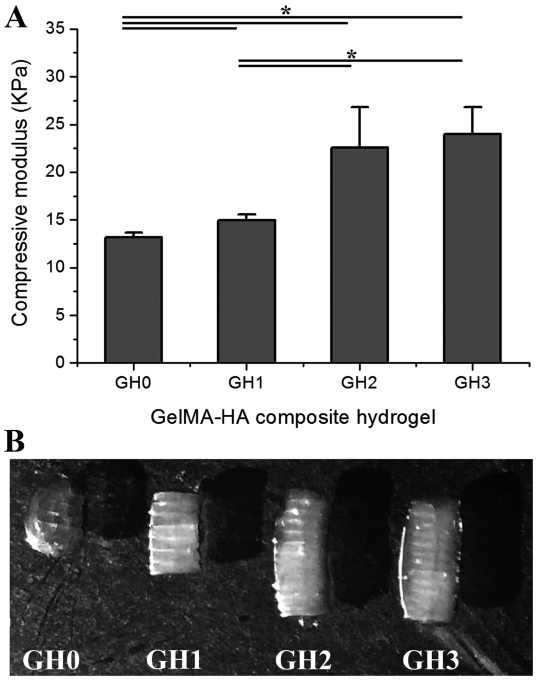

Figure 4. (A) Compressive moduli of the GelMA-based composite hydrogels (asterisk (*) indicates $p < 0.05$). (B) Phase contrast images of the sequentially assembled constructs by using the GH0, GH1, GH2, and GH3 microgels.

Figure 4B showed the sequentially assembled structures by use of the GH0, GH1, GH2, and GH3 microgel units, of which the number in the assembly increased from 5 to 13. In addition, during the assembling process, the GH0 was difficult to be assembled and its final structure was irregular while the others could be maintained well.

3.2. Cell Viability and Morphology in GelMA-Based Bulk Composite Hydrogel. The live/dead status, proliferation, and spreading of MG63s and HUVECs in GelMA-based bulk hydrogels are presented in Figures 5−7.

As can be seen from the CLSM images, both MG63s and HUVECs in GelMA−HA bulk hydrogels exhibited a high viability. As for MG63s, GH2 showed a significantly higher proliferation rate than the others on day 7 while GH3 showed a slower increase and a lower cell density (Figures 5A and 7A).

DOI: 10.1021/acsami.5b01433
ACS Appl. Mater. Interfaces 2015, 7, 10386−10394

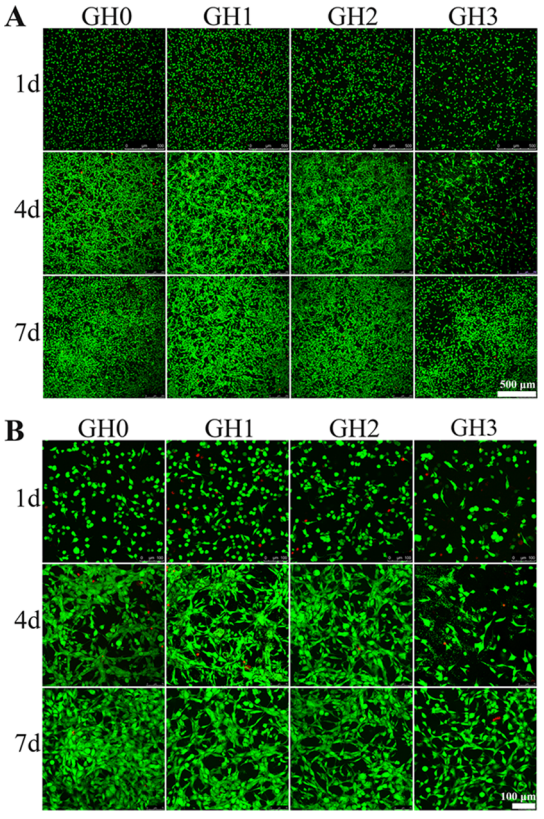

Figure 5. Confocal images of MG63s-laden bulk GelMA-based hydrogel after being cultured for 1, 4, and 7 days: (A) lower magnification and (B) higher magnification. Cell seeding density: 5×10^6 cells mL^{-1}. Scale bars: 500 (A) and 100 μm (B).

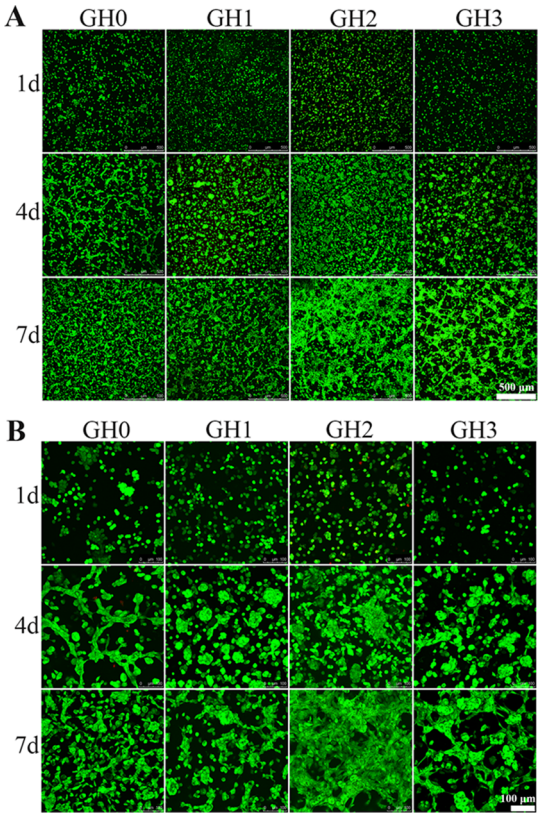

Figure 6. Confocal images of HUVECs-laden bulk GelMA-based hydrogel after being cultured for 1, 4, and 7 days: (A) lower magnification and (B) higher magnification. Cell seeding density: 5×10^6 cells mL^{-1}. Scale bars: 500 (A) and 100 μm (B).

The magnified images (Figure 5B) exhibited that cells in all four groups began to form extensions, although a portion of the cells still remained round after 1 day encapsulation. The number of spread cells and their spreading extension increased with the incubation time. Finally, cells in the composite hydrogels developed into a typical spindle shape, in which pseudopods were clearly visible. However, most cells in GH3 hydrogel remained in a round or restrained shape.

For HUVECs, an enhanced proliferation in GelMA−HA groups than the one in GelMA was observed, particularly in GH2, which showed a notably higher rate than the other two composite ones (Figures 6B and 7B). According to Figure 6B, HUVECs formed individual cell aggregations at day 4 and eventually developed into connected networks at day 7 (represented by GH2 and GH3).

Also, it should be noted that GH2 showed higher aggregation with a larger connected area. Nonetheless, few connected networks were found in GH0 and GH1. In addition, HUVECs in all groups exhibited its natural cobblestone shape as the culture time extended.

3.3. Construction and Characterization of Cell-Laden Osteon-Like System Based on the Composite Hydrogel.

According to the above characterizations of the serial GelMA−HA composites, group GH2 was the optimal selection to be utilized in the following modular construction due to its stable swelling behavior, relatively high mechanical rigidity, good assembly performance, and superior biocompatibility. As shown in Figure 8A, the osteon-like unit had a concentric double-ring structure with an inner diameter of 500 μm, a middle diameter of 1.2 mm, and an outer diameter of 2 mm and could be further manually assembled into a regular and tightly coupled assembly (Figure 8B). The perfusion test (Figure 8C) indicated the connective lumen embedded within the assembly.

Figure 8D−F displays cell distributions, proliferation, and morphologies of the coculture system in which HUEVCs was encapsulated in the inner ring while MG63s is in the outer ring. Both cells exhibited high viability and rapid growth, and the shapes of the microgel unit and assembly were preserved well. Cell morphologies were observed in Figure 8G−I. As the culture time was extended, both MG63s and HUVECs gradually spread into their spindle shape and cobblestone shape in the system, respectively. Nevertheless, cell density reached an extremely high level in hydrogel after 7 day encapsulation, making it indistinct to observe their morphologies.

Gene expressions of cell-related differentiation in the osteon-like assembly were detected and quantified by qRT-PCR (Figure 9). Cell (MG63s or HUVECs)-laden GelMA bulk hydrogel was used as the control group. In gene selection, OCN, COL-I, and ALP were chosen as markers for osteogenesis differentiation of MG63s while VEGF for angiogenesis differentiation of HUVECs. In all groups, all gene expressions dramatically increased with prolonged culture time (from day 4 to day 7). For bone-related genes, there was no significant difference between the GelMA−HA assembly and the bulk GelMA hydrogel for ALP and OCN expressions, while the COL-I expression was obviously enhanced in the assembly at the same time point. Interestingly, as to vascular-related gene VEGF, a significantly higher expression in the

DOI: 10.1021/acsami.5b01433
ACS Appl. Mater. Interfaces 2015, 7, 10386−10394

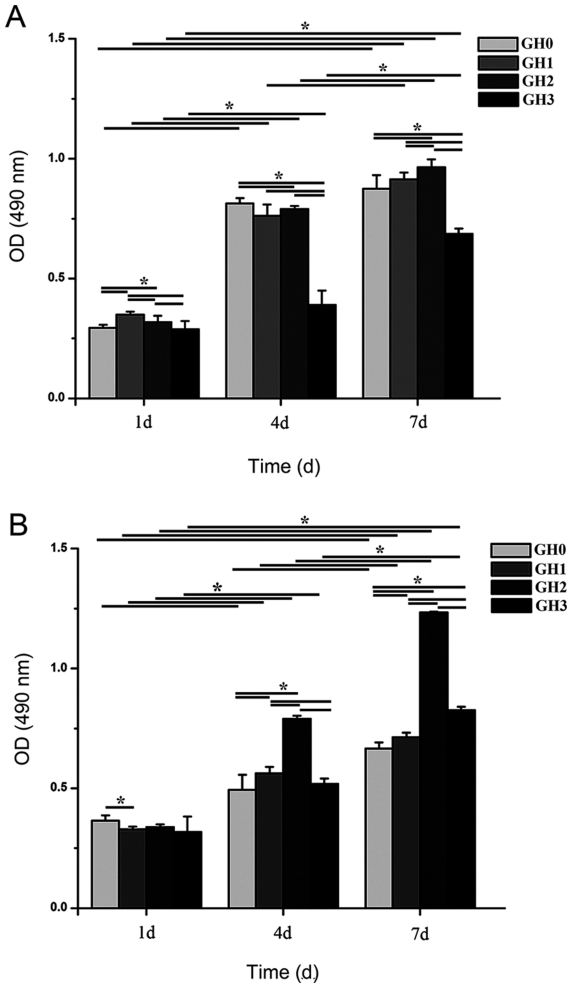

Figure 7. MTT analysis of the MG63s (A) and HUVECs (B) in the GelMA-based hydrogels after incubation for 1, 4, and 7 days (asterisk (*) indicates $p < 0.05$).

assembly than the one in the bulk hydrogel was observed on both time points.

4. DISCUSSION

Modular tissue engineering shows huge prospect in the regeneration of complex tissues. Selection of the scaffold material is the substantive factor to successful construction of the modular tissue. Given the requirements of the modular construction on molding, assembly, and biological function of the microscale unit, a desirable scaffold is supposed to possess the following features: arbitrary molding, high mechanical property, and biocompatibility.

In this article, we explored a photo-cross-linkable GelMA-templated HA composite hydrogel with advantages of both improved mechanical rigidity and cell bioactivity for modular construction of biomimetic osteon. Preparation of this multi-ingredient hydrogel was initiated by a collagen−HA combination system in natural bone matrix and to get the patternable property for modular biofabrication. To introduce HA into the GelMA template, we chose chemical synthesis of HA in the presence of Ca and P in GelMA solution (Figure 10).

As illustrated in Figure 10, there should be two HA formation mechanisms in GelMA network. One comes from the reactions between calcium ions and phosphate radicals free in GelMA network, which would result in homogeneous

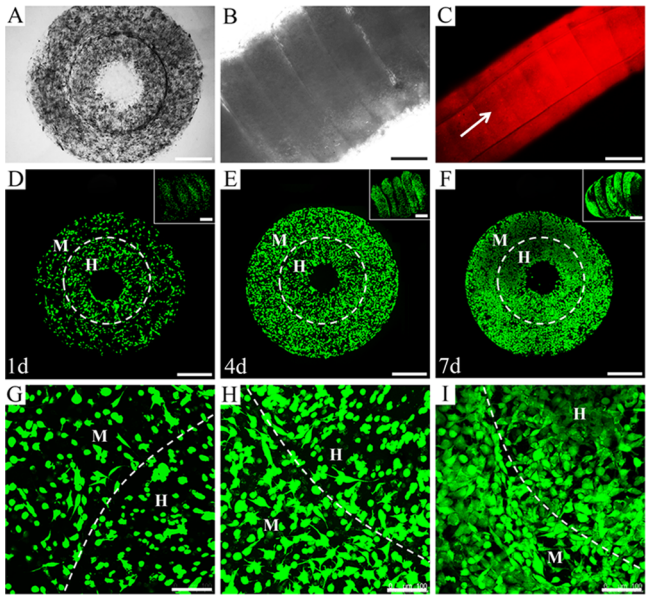

Figure 8. Characterization of osteon-like double-ring modules. (A, B) Phase-contrast images of a single unit and an assembly. (C) Fluorescent images under the Rhodamine (red) perfusion. (D−F) Confocal images of the cell-laden micropatterned unit for 1, 4, and 7 days, (insert) related assembly. (G−I) Higher magnification of confocal images. M stands for MG63s, and H stands for HUVECs. Cell seeding density: 5×10^6 cells mL^{-1}. Scale bars: 500 (A−F) and 100 μm (G−I).

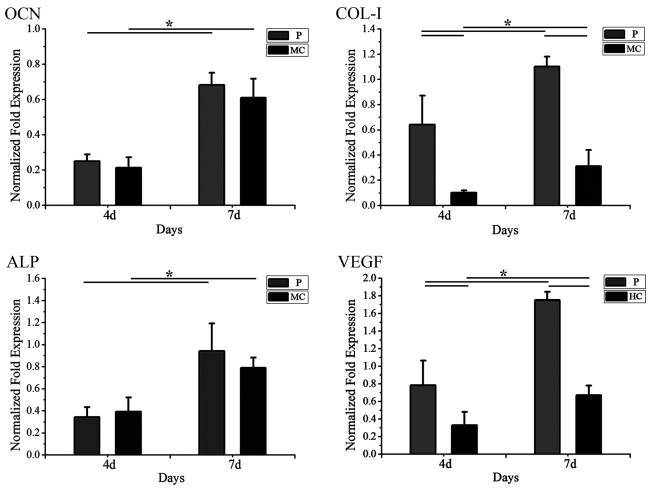

Figure 9. Quantitative genic expressions of MG63s and HUVECs in osteon-like assembly after 4 and 7 days' incubation by qRT-PCR (asterisk (*) indicates $p < 0.05$). P stands for MG63s and HUVECs in micropatterned GelMA−HA assembly. MC stands for MG63s in unpatterned GelMA hydrogel (MG63s only), and HC stands for HUVECs in unpatterned GelMA hydrogel (HUVECs only).

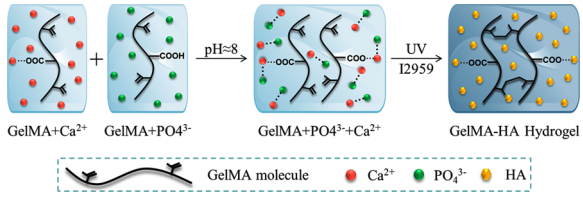

Figure 10. Schematic description of the mechanism of HA formation in GelMA network.

DOI: 10.1021/acsami.5b01433
ACS Appl. Mater. Interfaces 2015, 7, 10386−10394

formation of HA filling with spatial structure of the hydrogel network, and this should be a fundamental way of HA formation in GelMA network. The other one relies on the chemical combination of GelMA molecule and HA. According to the HA mineralization mechanism in natural bone matrix, molecular blocks of collagen play an important role to induce chemical bonding between calcium and phosphate, guiding HA in situ formation.[22,23] As a hydrolysis product of collagen, gelatin is believed to retain these molecular characteristics and possess potential abilities to guide HA precipitation in a calcium and phosphate coexisting system, and this has been demonstrated by previous reports about the fabrication of gelatin−HA nanofibers or nanocomposites.[20,21] On the basis of this fact, it could be inferred that this inducement also occurred in our GelMA−HA system. First, specific groups in GelMA molecules, such as the carboxyl group, would conjugate with the surrounding free calcium ions. Subsequently, phosphate radical would react with the calcium and finally induce the formation of HA, forming HA-integrated GelMA molecules. Similar inducement of HA precipitation by specific polymer chain template has been reported in previous studies.[24,25]

According to XRD, FTIR, HRTEM, and SEAD analysis, formation of HA was demonstrated. Due to the in situ precipitation and organic molecules inducing growth of HA, the as-received HA crystal was in submicro/nanoscale size with slight distortions of the crystal lattice in the progress of crystallization; thus, the crystallinity was relatively low, and the typical diffraction peaks of HA appeared broadened in XRD.[26] This is consistent with previous reports that this kind of apatite crystallization in organic media is a common phenomenon.[27] Moreover, thanks to the above-mentioned formation mechanism, both precipitation patterns of HA would result in its homogeneous distribution in GelMA network as confirmed by EDS analysis, SEM, and TEM images. Significantly, this homogeneity not only guaranteed the uniform physiochemical properties of the composite hydrogel but also improved its swelling, mechanical properties, as well as bioactivities.

Hydrogel swelling results from the molecular water absorption.[28] GelMA molecule is flexible, and it will cause an obvious network expansion when absorbing water, which means a high swelling ratio, while HA particles are rigid[24] and water absorption will only give rise to an ignorable volume change, presenting a low swelling ratio. Therefore, HA filling in GelMA network limited GelMA molecular expansion, leading to a decreased swelling ratio.

Furthermore, benefiting from the stiffness of HA and its homogeneous distribution, the composite hydrogel gained an enhanced mechanical strength with the ability to resist external compression force. Another reason for this enhancement should be attributed to the molecular precipitation of HA which rendered GelMA molecule strengthened rigidity. Nevertheless, when HA content increased from 2 to 3 w/v %, the hydrogel compression moduli showed no evidence of a corresponding strengthening. This might be due to excess formation of HA, which would lead to a heterogeneous compounding and incomplete gelation, failing to have a further promotional effect on hydrogel mechanics.

Both improved swelling and mechanical properties endowed the composite hydrogel better modular assembly performance as demonstrated by the sequential assembly since a low swelling level represents a small shape deformation which is conducive to stabilizing microgel assembly, and the enhanced stiffness offers the microgel an intact architecture, which is in favor of the assembling process.

More important, introducing HA into GelMA network stimulated cellular bioactivities of MG63s and HUVECs. To engineer biomimetic bone by modular assembly, the functional establishment of osteon would be a primary requirement. Focusing on this aim, MG63s and HUVECs were chosen to test the biocompatibility of the composite hydrogel for MG63s belongs to the human osteoblast cell line with a high potential of differentiation into bone,[29] and HUVECs belongs to the human endothelial cell line with great abilities to differentiate toward vascular tube.[30] Due to the cell-affinitive domains Arg-Gly-Asp (RGD) in GelMA molecules[31] and high bioactivity for osteo-related cell of HA,[32] MG63s showed satisfying growth status in composite hydrogel. In particular, a higher proliferation rate in GH2 than other groups was observed, indicating that the combination of GelMA and HA in GH2 provided the hydrogel with an optimal microenvironment mimicking natural bone matrices, better stimulating cell growth. This kind of positive response by HA-containing scaffold to enhance bone-related cell biological activities as compared to those by individual scaffold has been reported in other similar systems.[20,33] Unexpectedly, a decreased cell proliferation and restrained cell morphologies were observed in GH3, and this might result from an excess HA formation which might limit cell spreading in GelMA network.[6]

As to HUVECs, all composite hydrogels exhibited advantages in enhancing cellular activities than GelMA alone. Previous reports have demonstrated that microscale HA crystals possess high biocompatibility for vascular endothelium-related cell culture.[34] Therefore, the significant proliferation of HUVECs within the composite hydrogel can be attributed to a stimulative effect by HA. Interestingly, notable cell aggregations were observed in HA-containing groups, especially remarkable in GH2, indicating that addition of HA could promote cellular self-assembly. The cell aggregation is regarded to be in favor of cell−cell communication, stimulating cell activity, such as immigration and proliferation.[35] As a consequence, the abundant formation of cell aggregations in GH2 means a better cell functional establishment.

The above-mentioned results suggested that the novel GelMA−HA composite hydrogel was successfully prepared with both enhanced mechanical rigidity and improved cell biocompatibility and could be a potent alternative scaffold for modular tissue engineering. Further feasibility of constructing modular tissues was proved by biomimetic osteon fabrication and assembly.

Owing to the photo-cross-linking ability of GelMA, the composite could be lightly patternable into different geometries with controlled dimension.[3] On the basis of this property, concentric double-ring microgels construct was successfully fabricated with a lumen-contained osteon-like structure in which MG63s spatially distributed in the outer ring and HUVECs in the inner ring to mimic natural bone ECM and blood vessel-like microtubule relatively. This modular system architecturally and biologically embodied a simplified model of natural osteon. The successful construction and perfusion test again proved the perfect assembling performance and structure preserving of the microgels by use of GelMA−HA composite.

During the incubation period, both MG63s and HUVECs populating in this modular system exhibited a satisfing growth status as expected. On one hand, this is undoubtedly related to the high bioactivity of GelMA−HA composite; on the other

DOI: 10.1021/acsami.5b01433
ACS Appl. Mater. Interfaces 2015, 7, 10386−10394

hand, the connective channel embedded within the assembly also contributed a promotion effect to cellular behaviors for such connective channels within the scaffold can enhance cell survival by guaranteeing adequate oxygenation, nutrient delivery, and removal of waste products.[36]

Finally, osteogenic differentiation of MG63s by expression of OCN, COL-I, and ALP and angiogenic differentiation of HUVECs by expression of VEGF further confirmed the functional establishment of bone and vascular in the assembly. These genes are considered as important markers for bone/vascular forming cell and have been popularly selected to evaluate the performance of the scaffold in related-tissue forming process.[37,38] Therefore, the results revealed an inducement of cellular differentiation by the composite hydrogel. Of special note was the observation that COL-I expression as well as VEGF in the modular system was significantly higher than the one in bulk GelMA hydrogel. This up-regulation is partially attributed to GelMA and HA, which are well known to stimulate bone/vascular-derived cell bioactivities.[31,39,40] Furthermore, the homogeneous combination of GelMA and HA provided the hydrogel with an efficient composite structure mimicing the inorganic−organic natural system in bone; thus, it could enhance cell−cell and cell−matrix responses, resulting in increased cellular secretions. Another considerable reason comes from our modular design which enables coculture of MG63s and HUVECs. Numerous studies on multitype cell cocultivation have been demonstrated to achieve enhanced cellular differentiation-related expression which deeply relies on the interactive biological stimulation between cells.[31,41] For example, during the bone formation process, bone forming cell differentiation can be stimulated by introducing a vascular forming cell system which in the meanwhile can be stimulated by surrounding bone cell−ECM environment to develop into blood vessel formation.[42,43] Therefore, this interaction also existed between MG63s and HUVECs in our modular system and promoted cell-specific differentiation.

In summary, the above results demonstrated that the modular fabrication of biomimetic osteon was successfully conducted by utilizing the novel GelMA−HA composite. This construction was dependent on the composite hydrogel with advantages of both high mechanical stiffness for modular assembly performance and prominent biocompatibility for cell growth and functional expressions. Significantly, these results also indicate that the photo-cross-linkable character of the composite allows for spatial control over the polymerization reaction and makes the hydrogel system particularly attractive for the fabrication of other complex 3D natural tissues which are comprised of repeating functional units, such as lobule in the liver.[12] Therefore, this multi-ingredient hydrogel holds prodigious potential to be developed as a competitive candidate in modular tissue engineering. However, compared with traditional bone-repairing scaffolds used in clinics, the mechanical moduli of the composite GH series are low, limiting its application presently. This disadvantage is expected to be overcome by rapid tissue regeneration through optimized material bioactivity and biomimetic tissue construction. Thus, this composite material needs to be further optimized, and relevant research is progressing in our laboratory.

5. CONCLUSION

Herein, we demonstrated the successful fabrication of a novel 3D GelMA−HA composite hydrogel. This composite hydrogel was proved to possess a stronger mechanical property, a more stable swelling behavior, and better biocompatibility than the GelMA individual equivalent. Utilization of the composite in constructing biomimetic osteon for bone regeneration on the basis of photolithography exhibited its great capabilities in promoting cell growth and specific cellular differentiation. These results endow this composite system a prospective application in modular tissue engineering for bone reconstruction.

■ ASSOCIATED CONTENT

Supporting Information

Schematic illustration of fabricating the hydrogel disc, schematic illustration of fabricating the osteon-like double-ring microgel and assembly, and energy-dispersive spectroscopy (EDS) analysis of the GH1, -2, and -3 samples. The Supporting Information is available free of charge on the ACS Publications website at DOI: 10.1021/acsami.5b01433.

■ AUTHOR INFORMATION

Corresponding Author

*Tel.: 86-28-85410703. Fax: 86-28-85410246. E-mail: hsfan@scu.edu.cn.

Author Contributions

†Yicong Zuo and Xiaolu Liu contributed equally. The manuscript was written through contributions of all authors. All authors have given approval to the final version of the manuscript.

Notes

The authors declare no competing financial interest.

■ ACKNOWLEDGMENTS

This work was supported by the National Natural Science Foundation of China (Contract Grant Nos. 51273121, 51473098, 51373105, and 81190131) and National Basic Research Program of China (Contract Grant No. 2011CB606201).

■ REFERENCES

(1) Gauvin, R.; Khademhosseini, A. Microscale Technologies and Modular Approaches for Tissue Engineering: Moving toward the Fabrication of Complex Functional Structures. *ACS Nano* **2011**, *5*, 4258−4264.

(2) Dean, D. M.; Napolitano, A. P.; Youssef, J.; Morgan, J. R. Rods, Tori, and Honeycombs: The Directed Self-assembly of Microtissues with Prescribed Microscale Geometries. *FASEB J.* **2007**, *21*, 4005−4012.

(3) Du, Y.; Lo, E.; Ali, S.; Khademhosseini, A. Directed Assembly of Cell-Laden Microgels for Fabrication of 3D Tissue Constructs. *Proc. Natl. Acad. Sci. U.S.A.* **2008**, *105*, 9522−9527.

(4) L'heureux, N.; Pâquet, S.; Labbé, R.; Germain, L.; Auger, F. A. A Completely Biological Tissue-engineered Human Blood Vessel. *FASEB J.* **1998**, *12*, 47−56.

(5) Mironov, V.; Boland, T.; Trusk, T.; Forgacs, G.; Markwald, R. R. Organ Printing: Computer-aided Jet-based 3D Tissue Engineering. *Trends Biotechnol.* **2003**, *21*, 157−161.

(6) Lee, K. Y.; Mooney, D. J. Hydrogels for Tissue Engineering. *Chem. Rev.* **2001**, *101*, 1869−1880.

(7) Nguyen, K. T.; West, J. L. Photopolymerizable Hydrogels for Tissue Engineering Applications. *Biomaterials* **2002**, *23*, 4307−4314.

(8) Zuo, Y.; Xiao, W.; Chen, X.; Tang, Y.; Luo, H.; Fan, H. Bottom-up Approach to Build Osteon-like Structure by Cell-laden Photo-crosslinkable Hydrogel. *Chem. Commun.* **2012**, *48*, 3170−3172.

DOI: 10.1021/acsami.5b01433
ACS Appl. Mater. Interfaces 2015, 7, 10386−10394

(9) Zamanian, B.; Masaeli, M.; Nichol, J. W.; Khabiry, M.; Hancock, M. J.; Bae, H.; Khademhosseini, A. Interface-directed Self-assembly of Cell-laden Microgels. *Small* **2010**, *6*, 937−944.
(10) Xu, F.; Finley, T. D.; Turkaydin, M.; Sung, Y.; Gurkan, U. A.; Yavuz, A. S.; Guldikenb, R. O.; Demirci, U. The Assembly of Cell-encapsulating Microscale Hydrogels Using Acoustic Waves. *Biomaterials* **2011**, *32*, 7847−7855.
(11) Zorlutuna, P.; Annabi, N.; Camci-Unal, G.; Nikkhah, M.; Cha, J. M.; Nichol, J. W.; Manbachi, A.; Bae, H.; Chen, S.; Khademhosseini, A. Microfabricated Biomaterials for Engineering 3D Tissues. *Adv. Mater.* **2012**, *24*, 1782−1804.
(12) Tsang, V. L.; Chen, A. A.; Cho, L. M.; Jadin, K. D.; Sah, R. L.; DeLong, S.; West, J. L.; Bhatia, S. N. Fabrication of 3D Hepatic Tissues by Additive Photopatterning of Cellular Hydrogels. *FASEB J.* **2007**, *21*, 790−801.
(13) Ibusuki, S.; Halbesma, G. J.; Randolph, M. A.; Redmond, R. W.; Kochevar, I. E.; Gill, T. J. Photochemically Cross-linked Collagen Gels as Three-dimensional Scaffolds for Tissue Engineering. *Tissue Eng.* **2007**, *13*, 1995−2001.
(14) Möller, L.; Krause, A.; Dahlmann, J.; Gruh, I.; Kirschning, A.; Dräger, G. Preparation and Evaluation of Hydrogel-composites from Methacrylated Hyaluronic Acid, Alginate, and Gelatin for Tissue Engineering. *Int. J. Artif. Organs* **2011**, *34*, 93−102.
(15) Nichol, J. W.; Koshy, S. T.; Bae, H.; Hwang, C. M.; Yamanlar, S.; Khademhosseini, A. Cell-laden Microengineered Gelatin Methacrylate Hydrogels. *Biomaterials* **2010**, *31*, 5536−5544.
(16) Augat, P.; Schorlemmer, S. The Role of Cortical Bone and Its Microstructure in Bone Strength. *Age Ageing* **2006**, *35*, 27−31.
(17) Wahl, D.; Czernuszka, J. Collagen-hydroxyapatite Composites for Hard Tissue Repair. *Eur. Cell. Mater.* **2006**, *11*, 43−56.
(18) Liu, H.; Cheng, J.; Chen, F.; Hou, F.; Bai, D.; Xi, P.; Zeng, Z. Biomimetic and Cell-mediated Mineralization of Hydroxyapatite by Carrageenan Functionalized Graphene Oxide. *ACS Appl. Mater. Interfaces* **2014**, *6*, 3132−3140.
(19) Woodard, J. R.; Hilldore, A. J.; Lan, S. K.; Park, C.; Morgan, A. W.; Eurell, J. A.; Clark, S. G.; Wheeler, M. B.; Jamison, R. D.; Wagoner Johnson, A. J. The Mechanical Properties and Osteoconductivity of Hydroxyapatite Bone Scaffolds with Multi-scale Porosity. *Biomaterials* **2007**, *28*, 45−54.
(20) Chang, M. C.; Ko, C. C.; Douglas, W. H. Preparation of Hydroxyapatite-gelatin Nanocomposite. *Biomaterials* **2003**, *24*, 2853−2862.
(21) Chiu, C. K.; Ferreira, J.; Luo, T. J. M.; Geng, H.; Lin, F. C.; Ko, C. C. Direct Scaffolding of Biomimetic Hydroxyapatite-gelatin Nanocomposites Using Aminosilane Cross-linker for Bone Regeneration. *J. Mater. Sci: Mater. Med.* **2012**, *23*, 2115−2126.
(22) Zhang, W.; Huang, Z. L.; Liao, S. S.; Cui, F. Z. Nucleation Sites of Calcium Phosphate Crystals during Collagen Mineralization. *J. Am. Ceram. Soc.* **2003**, *86*, 1052−1054.
(23) Rhee, S. H.; Lee, J. D.; Tanaka, J. Nucleation of Hydroxyapatite Crystal through Chemical Interaction with Collagen. *J. Am. Ceram. Soc.* **2000**, *83*, 2890−2892.
(24) Zhang, H.; Liu, M.; Fan, H.; Zhang, X. An Efficient Method to Synthesize Carbonated Nano Hydroxyapatite Assisted by Poly (ethylene glycol). *Mater. Lett.* **2012**, *75*, 26−28.
(25) Liao, S.; Watari, F.; Uo, M.; Ohkawa, S.; Tamura, K.; Wang, W.; Cui, F. The Preparation and Characteristics of a Carbonated Hydroxyapatite/Collagen Composite at Room Temperature. *J. Biomed. Mater. Res. B: Appl. Biomater.* **2005**, *74*, 817−821.
(26) Murugan, R.; Ramakrishna, S. Aqueous Mediated Synthesis of Bioresorbable Nanocrystalline Hydroxyapatite. *J. Cryst. Growth* **2005**, *274*, 209−213.
(27) Weiner, S.; Addadi, L. Design Strategies in Mineralized Biological Materials. *J. Mater. Chem.* **1997**, *7*, 689−702.
(28) Ganji, F.; Vasheghani-Farahani, S.; Vasheghani-Farahani, E. Theoretical Description of Hydrogel Swelling: A Review. *Iran. Polym. J.* **2010**, *19*, 375−398.
(29) Martin, J.; Dean, D.; Cochran, D.; Simpson, J.; Boyan, B.; Schwartz, Z. Proliferation, Differentiation, and Protein Synthesis of Human Osteoblast-like Cells (MG63) Cultured on Previously Used Titanium Surfaces. *Clin. Oral Implants Res.* **1996**, *7*, 27−37.
(30) Nakatsu, M. N.; Sainson, R. C.; Aoto, J. N.; Taylor, K. L.; Aitkenhead, M.; Pérez-del-Pulgar, S.; Carpenter, P. M.; Hughes, C. C. Angiogenic Sprouting and Capillary Lumen Formation Modeled by Human Umbilical Vein Endothelial Cells (HUVEC) in Fibrin Gels: The Role of Fibroblasts and Angiopoietin-1. *Microvasc. Res.* **2003**, *66*, 102−112.
(31) Chen, Y. C.; Lin, R. Z.; Qi, H.; Yang, Y.; Bae, H.; Melero-Martin, J. M.; Khademhosseini, A. Functional Human Vascular Network Generated in Photocrosslinkable Gelatin Methacrylate Hydrogels. *Adv. Funct. Mater.* **2012**, *22*, 2027−2039.
(32) Ripamonti, U. Osteoinduction in Porous Hydroxyapatite Implanted in Heterotopic Sites of Different Animal Models. *Biomaterials* **1996**, *17*, 31−35.
(33) Anderson, J. M.; Patterson, J. L.; Vines, J. B.; Javed, A.; Gilbert, S. R.; Jun, H. W. Biphasic Peptide Amphiphile Nanomatrix Embedded with Hydroxyapatite Nanoparticles for Stimulated Osteoinductive Response. *ACS Nano* **2011**, *5*, 9463−9479.
(34) Sha, J.; Yan, Z.; Cheng, G. C.; Weil, X. Y.; Tao, Y.; Li, Y. M.; Luo, L. In-vitro Seeding of Human Umbilical Cord Vein Endothelial Cells on Hydroxyapatite for Mechanical Heart Valve Applications. *J. Heart Valve Dis.* **2010**, *19*, 506−512.
(35) Kelm, J. M.; Fussenegger, M. Microscale Tissue Engineering Using Gravity-enforced Cell Assembly. *Trends Biotechnol.* **2004**, *22*, 195−202.
(36) Huang, H.; Oizumi, S.; Kojima, N.; Niino, T.; Sakai, Y. Avidin−biotin Binding-based Cell Seeding and Perfusion Culture of Liver-derived Cells in a Porous Scaffold With a Three-dimensional Interconnected Flow-channel Network. *Biomaterials* **2007**, *28*, 3815−3823.
(37) Sun, J.; Xiao, W.; Tang, Y.; Li, K.; Fan, H. Biomimetic Interpenetrating Polymer Network Hydrogels Based on Methacrylated Alginate and Collagen for 3D Pre-osteoblast Spreading and Osteogenic Differentiation. *Soft Matter* **2012**, *8*, 2398−2404.
(38) Ferrara, N.; Gerber, H. P.; LeCouter, J. The Biology of VEGF and Its Receptors. *Nat. Med.* **2003**, *9*, 669−676.
(39) Lin, K.; Xia, L.; Gan, J.; Zhang, Z.; Chen, H.; Jiang, X.; Chang, J. Tailoring the Nanostructured Surfaces of Hydroxyapatite Bioceramics to Promote Protein Adsorption, Osteoblast Growth, and Osteogenic Differentiation. *ACS Appl. Mater. Interfaces* **2013**, *5*, 8008−8017.
(40) Furuzono, T.; Masuda, M.; Okada, M.; Yasuda, S.; Kadono, H.; Tanaka, R.; Miyatake, K. Increase in Cell Adhesiveness on a Poly (ethylene terephthalate) Fabric by Sintered Hydroxyapatite Nanocrystal Coating in the Development of an Artificial Blood Vessel. *ASAIO J.* **2006**, *52*, 315−320.
(41) Harimoto, M.; Yamato, M.; Hirose, M.; Takahashi, C.; Isoi, Y.; Kikuchi, A.; Okano, T. Novel Approach for Achieving Double-layered Cell Sheets Co-culture: Overlaying Endothelial Cell Sheets onto Monolayer Hepatocytes Utilizing Temperature-responsive Culture Dishes. *J. Biomed. Mater. Res.* **2002**, *62*, 464−470.
(42) Unger, R. E.; Sartoris, A.; Peters, K.; Motta, A.; Migliaresi, C.; Kunkel, M.; Bulnheim, U.; Rychly, J.; Kirkpatrick, C. J. Tissue-like Self-assembly in Cocultures of Endothelial Cells and Osteoblasts and the Formation of Microcapillary-like Structures on Three-Dimensional Porous Biomaterials. *Biomaterials* **2007**, *28*, 3965−3976.
(43) Street, J.; Bao, M.; Bunting, S.; Peale, F. V.; Ferrara, N.; Steinmetz, H.; Hoeffel, J.; Cleland, J. L.; Daugherty, A.; van Bruggen, N.; Redmond, H. P.; Carano, R. A.; Filvaroff, E. H. Vascular Endothelial Growth Factor Stimulates Bone Repair by Promoting Angiogenesis and Bone Turnover. *Proc. Natl. Acad. Sci. U.S.A.* **2002**, *99*, 9656−9661.

DOI: 10.1021/acsami.5b01433
ACS Appl. Mater. Interfaces 2015, 7, 10386−10394